COLOR

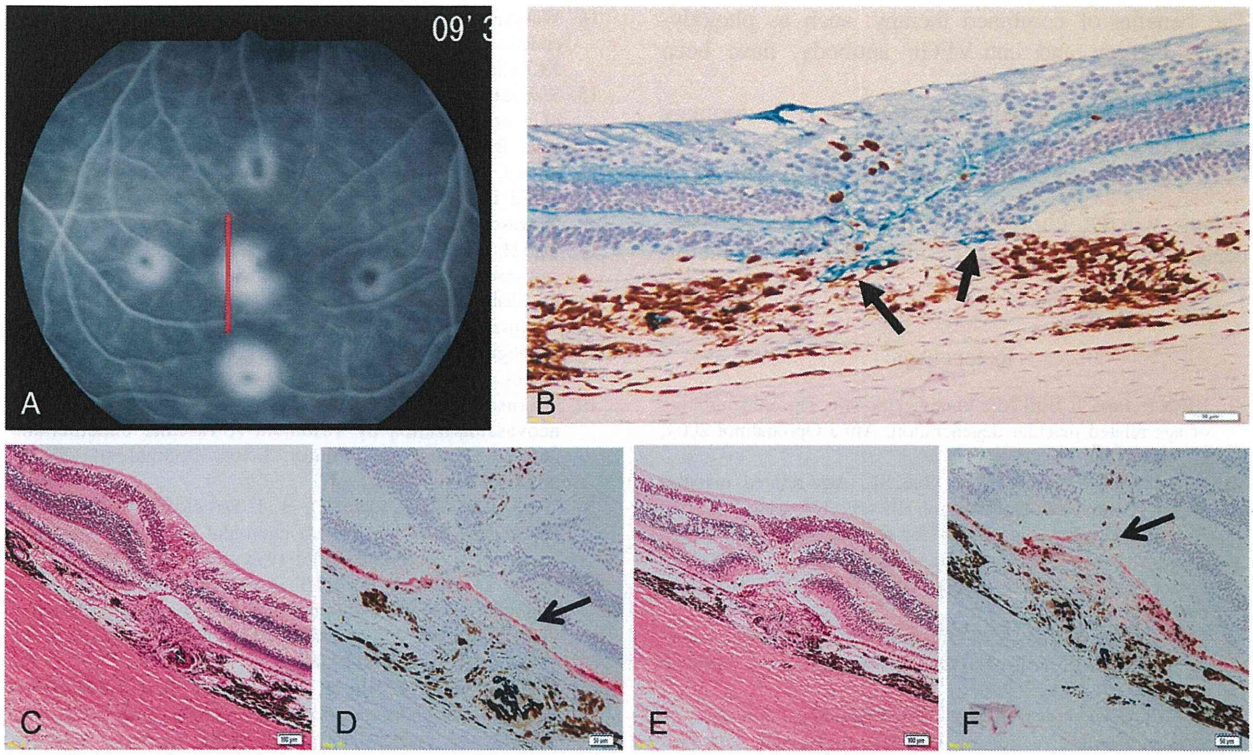

Fig. 5. Fluorescein angiograms 4 weeks after laser application or vehicle injection are shown. **A.** Immunohistochemistry for vasohibin-1 (**B**), the same eye as shown in (**A**) at the red line, is shown. Arrows indicate vasohibin-1 labeling. Vasohibin-1 expression is concentrated on the vessels around the CNV (arrows), but markedly less than in the CNV. Vaoshibin-1 expression was observed at active CNV (red line in **A**). The subretinal space is an artifact of histologic processing. Cytokeratin labeling is also shown with vasohibin-treated eye (**D**) and vehicle-treated eye (**F**). Arrows show labeling of cytokeratin. Bar = 50 μm. **C** and **E.** Hematoxylin and eosin staining of vasohibin-1–treated and vehicle-treated eyes, respectively, are shown. Bar = 100 μm. Cytokeratin labeling shows that retinal pigment epithelium covers CNV in the vasohibin-1–treated eyes (**D**), and a disruption of cytokeratin labeling is observed in vehicle-treated eye (**F**).

Hosaka et al[29] reported that exogenous vasohibin-1 blocked angiogenesis and maturation of not only the cancerous tissue but also the surrounding vessels and, thus, enhanced the antitumor effects of vasohibin-1. Intravitreal injection of vasohibin-1 may also suppress angiogenesis in CNVs by the same mechanism.

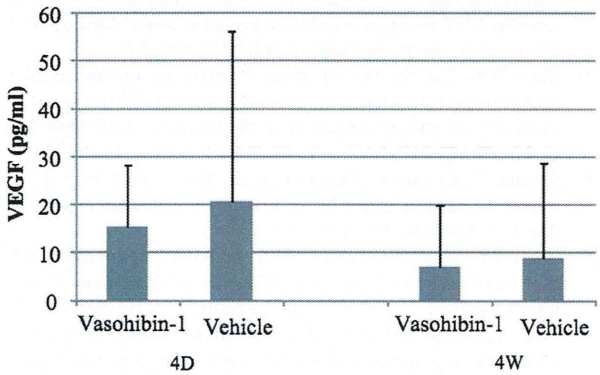

Fig. 6. Concentration of VEGF in aqueous in laser-treated monkey eyes 4 days and 4 weeks after laser application is shown. Vertical axis shows VEGF concentration in picograms per milliliter, and horizontal axis is the day of examination. Vascular endothelial growth factor in vasohibin-1–treated eyes (blue boxes) and vehicle-treated eyes (red boxes) show no significant difference at any times.

The amount of VEGF in the aqueous in the vasohibin-1–treated eyes did not differ from that in vehicle-treated eyes. Thus, Zhou et al[30] reported that external vasohibin-1 had no effect on the level of VEGF when they used adenovirus encoding human vasohibin-1 on mouse corneal neovascularization induced by alkali burn. They also reported that vasohibin-1 may downregulate the VEGF receptor 2 (VEGFR2). Shen et al[16] also reported a downregulation of VEGFR2 by vasohibin-1 during mouse ischemic retinopathy. Our previous studies have also shown a downregulation of VEGFR2 by external vasohibin-1 in laser-induced mouse CNVs.[19] Thus, vasohibin-1 may reduce the activity of a CNV by partially downregulating VEGFR2 in the eyes. If this is correct, vasohibin-1 may not affect the favorable aspects of VEGF such as its neuroprotective effect,[31] especially if VEGF works through VEGFR1 rather than VEGFR2. Vasohibin-1 also can be used with anti-VEGF antibody for CNV therapy.

The benefits of combined therapy, such as photodynamic therapy and anti-VEGF antibody, have been discussed.[27]

In conclusion, intravitreal vasohibin-1 in monkey eyes is safe and can reduce the activity of laser-induced CNVs and thus preserve the function of the macula.

Key words: choroidal neovascularization, laser-induced, monkey, vascular endothelial growth factor, vasohibin-1.

References

1. Klein R, Peto T, Bird AC, Vannewkirk MR. The epidemiology of age-related macular degeneration. Am J Ophthalmol 2004; 137:486–495.
2. Bressler NM, Bressler SB, Fine SL. Age-related macular degeneration. Surv Ophthalmol 1998;32:375–413.
3. Argon laser photocoagulation for neovascular maculopathy. Three-year results from randomized clinical trials Macular Photocoagulation Study Group. Arch Ophthalmol 1986;104: 694–701.
4. Thomas MA, Grand MG, Williams DF, et al. Surgical management of subfoveal choroidal neovascularization. Ophthalmology 1992;99:952–968.
5. Eckardt C, Eckardt U, Conrad HG. Macular rotation with and without counter-rotation of the globe in patients with age-related macular degeneration. Graefes Arch Clin Exp Ophthalmol 1999;237:313–325.
6. Reichel E, Berrocal AM, Ip M, et al. Transpupillary thermotherapy of occult subfoveal choroidal neovascularization in patients with age-related macular degeneration. Ophthalmology 1999; 106:1908–1914.
7. Photodynamic therapy of subfoveal choroidal neovascularization in age-related macular degeneration with verteporfin: one year results of 2 randomized clinical trials-TAP report Treatment of Age-related Macular Degeneration with Photodynamic Therapy (TAP). Study Group. Arch Ophthalmol 1999;117:1329–1345.
8. Grisanti S, Tatar O. The role of vascular endothelial growth factor and other endogenous interplayers in age-related macular degeneration. Prog Retin Eye Res 2008;27:372–390.
9. Miller JW, Adamis AP, Shima DT, et al. Vascular endothelial growth factor/vascular permeability factor is temporally and spatially correlated with ocular angiogenesis in a primate model. Am J Pathol 1994;145:574–584.
10. Krzystolik MG, Afshari MA, Adamis AP, et al. Prevention of experimental choroidal neovascularization with intravitreal anti-vascular endothelial growth factor antibody fragment. Arch Ophthalmol 2002;120:338–346.
11. Rosenfeld PJ, Brown DM, Heier JS, et al. Ranibizumab for neovascular age-related macular degeneration. N Engl J Med 2006;355:1419–1431.
12. Pilli S, Kotsolis A, Spaide RF, et al. Endophthalmitis associated with intravitreal anti-vascular endothelial growth factor therapy injections in an office setting. Am J Ophthalmol 2008;145:879–882.
13. Lux A, Llacer H, Heussen FMA, Joussen AM. Non-responders to bevacizumab (Avastin) therapy of choroidal neovascular lesions. Am J Ophthalmol 2007;91:1318–1322.
14. Watanabe K, Hasegawa Y, Yamashita H, et al. Vasohibin as an endothelium-derived negative feedback regulator of angiogenesis. J Clin Invest 2004;114:898–907.
15. Shimizu K, Watanabe K, Yamashita H, et al. Gene regulation of a novel angiogenesis inhibitor, vasohibin, in endothelial cells. Biochem Biophys Res Commun 2005;327:700–706.
16. Shen J, Yang X, Xiao WH, et al. Vasohibin is up-regulated by VEGF in the retina and suppresses VEGF receptor 2 and retinal neovascularization. FASEB J 2006;20:723–725.
17. Sato H, Abe T, Wakusawa R, et al. Vitreous levels of vasohibin-1 and vascular endothelial growth factor in patients with proliferative diabetic retinopathy. Diabetologia 2009;52:359–361.
18. Wakusawa R, Abe T, Sato H, et al. Expression of vasohibin, an antiangiogenic factor, in human choroidal neovascular membranes. Am J Ophthalmol 2008;146:235–243.
19. Wakusawa R, Abe T, Sato H, et al. Suppression of choroidal neovascularization by vasohibin-1, vascular endothelium-derived angiogenic inhibitor. Invest Ophthalmol Vis Sci 2011;52:3272–3280.
20. Tobe T, Ortega S, Luna JD, et al. Targeted disruption of the FGF2 gene does not prevent choroidal neovascularization in a murine model. Am J Pathol 1998;153:1641–1646.
21. Heishi T, Hosaka T, Suzuki Y, et al. Endogenous angiogenesis inhibitor vasohibin1 exhibits broad-spectrum antilymphangiogenic activity and suppresses lymph node metastasis. Am J Pathol 2010;176:1950–1958.
22. Krzystolik MG, Afshari MA, Adamis AP, et al. Prevention of experimental choroidal neovascularization with intravitreal anti-vascular endothelial growth factor antibody fragment. Arch Ophthalmol 2002;120:338–346.
23. Miyake Y, Yanagida K, Yagasaki K, et al. Subjective scotometry and recording of local electroretinogram and visual evoked response. System with television monitor of the fundus. Jpn J Ophthalmol 1981;25:439–448.
24. Kondo M, Ueno S, Piao CH, et al. Comparison of focal macular cone ERGs in complete-type congenital stationary night blindness and APB-treated monkeys. Vision Res 2008;48: 273–280.
25. Hogan MJ, Kimura SJ, Thygeson P. Signs and symptoms of uveitis. I. Anterior uveitis. Am J Ophthalmol 1959;47:155–170.
26. Zhang M, Zhang J, Yan M, et al. Recombinant anti-vascular endothelial growth factor fusion protein efficiently suppresses choroidal neovascularization in monkeys. Mol Vision 2008;14:37–49.
27. Husain D, Kim I, Gauthier D, et al. Safety and efficacy of intravitreal injection of ranibizumab in combination with verteporfin PDT on experimental choroidal neovascularization in the monkey. Arch Ophthalmol 2005;123:509–516.
28. Shen WY, Lee SY, Yeo I, et al. Predilection of the macular region to high incidence of choroidal neovascularization after intense laser photocoagulation in the monkey. Arch Ophthalmol 2004;122:353–360.
29. Hosaka T, Kimura H, Heishi T, et al. Vasohibin-1 expression in endothelium of tumor blood vessels regulates angiogenesis. Am J Pathol 2009;175:430–439.
30. Zhou SY, Xie ZL, Xiao O, et al. Inhibition of mouse alkali burn induced-corneal neovascularization by recombinant adenovirus human vasohibin-1. Mol Vision 2010;16:1389–1398.
31. Alon T, Hemo I, Itin A, et al. Vascular endothelial growth factor acts as a survival factor for newly formed retinal vessels and has implications for retinopathy of prematurity. Nat Med 1995;1:1024–1028.

Chapter 40
Vasohibin-1 and Retinal Pigment Epithelium

Yumi Ishikawa, Nobuhiro Nagai, Hideyuki Onami, Norihiro Kumasaka, Ryosuke Wakusawa, Hikaru Sonoda, Yasufumi Sato, and Toshiaki Abe

Keywords Vasohibin • VEGF • Retinal pigment epithelium • Hypoxia • Cell dynamics • Cobalt chloride

40.1 Introduction

Choroidal neovascularization (CNV) leads to subretinal hemorrhages, exudative lesions, serous retinal detachment, and disciform scars in patients with age-related macular degeneration (AMD) (Bressler et al. 1998). Vascular endothelial growth factor (VEGF), a pro-angiogenic factor, plays a major role in the development of CNV (Spilsbury et al. 2000). Recently, anti-VEGF treatment for patients with AMD has developed and reported good results (Krzystolik et al. 2002; Rosenfeld et al. 2006). However, there are many problems, such as repeated intravitreal injections, side effects (Pilli et al. 2008), suppression of the important physiological VEGF function (Alon et al. 1995), and further not all patients respond well to this therapy (Lux et al. 2007). Vasohibin-1 is a VEGF-inducible gene in human cultured endothelial cells (ECs) with antiangiogenic properties (Watanabe et al. 2004; Sonoda et al. 2006). Vasohibin-1 is induced by several pro-angiogenic factors such as VEGF and

Y. Ishikawa • N. Nagai • H. Onami • N. Kumasaka • R. Wakusawa • T. Abe (✉)
Division of Clinical Cell Therapy, United Center for Advanced Research and Translational Medicine (ART), Tohoku University Graduate School of Medicine, 1-1 Seiryoumachi Aobaku Sendai, Miyagi, Japan
e-mail: toshi@oph.med.tohoku.ac.jp

H. Sonoda
Discovery Research Laboratories, Shionogi and Co. Ltd, Osaka, Japan

Y. Sato
Department of Vascular Biology, Institute of Development, Aging, and Cancer, Tohoku University Graduate School of Medicine, Miyagi, Japan

M.M. LaVail et al. (eds.), *Retinal Degenerative Diseases*, Advances in Experimental Medicine and Biology 723, DOI 10.1007/978-1-4614-0631-0_40,

basic fibroblast growth factor (bFGF) (Watanabe et al. 2004). We showed that the vasohibin-1/VEGF ratio might play a role for clinical significance of CNV in patients with AMD using surgically excised CNV membranes (Wakusawa et al. 2008). The membranes included not only ECs but also retinal pigment epithelium (RPE). In this report, we examined the effects of vasohibin-1 on RPE.

40.2 Methods

40.2.1 RPE Preparation

We used commercially available rat RPE cell line, RPE-J. RPE-J was cultured in DMEM/F-12 medium with 4% fetal bovine serum (FBS; Sigma, St. Louis MO) with 5% CO_2 supply at 33°C. Human vasohibin-1 cDNA with antineomycin gene vector was transduced into RPE-J as we previously reported (Abe et al. 2008). Cells that were stably introduced the vector were selected by antibiotics. We selected 18 clones on both vasohibin-1 cDNA and only vector-transduced RPE-Js. Cobalt chloride (100–300 μM) and low glucose (0–100 μM) and oxygen supply (2%) were used for hypoxic stress. Vasohibin-1 was supplied from Shionogi and Co. Ltd, Osaka, Japan and VEGF and other chemicals were purchased from Wako (Tokyo Japan).

40.2.2 Real-Time RPE Impedance Analysis and MTS Assay

Dynamic cellular biology of the cultured RPE was monitored using Real-Time Cell Analyzer (RTCA), xCELLigence System (Roche Applied Science, Mannheim, Germany). The system evaluates cellular events in real time measuring electrical impedance at an electrode/solution interface at the bottom of cell culture plates. The system provides cell number, viability, morphology, and adhesion described as Cell Index (CI). RPE proliferation was also evaluated by 3-(4, 5-dimethylthiazol-2-yl)-5-(3-carboxymethoxyphenyl)-2-(4-sulfophenyl)-2H-tetrazolium, inner salt (MTS) assay, and counting cell number for each condition.

40.2.3 Extraction of mRNA, cDNA Generation, Reverse-Transcriptase, and Real-Time Polymerase Chain Reaction (RT-PCR)

mRNA was extracted and cDNAs were generated from the cells according to the manufacturer's instructions (Pharmacia Biotech Inc., Uppsala, Sweden). Semiquantitative real-time PCR was carried out by the primer sets described below (LightCycleST300:Roche, Basel, Swiss). The sequences were 5′-TCT GCT CTC

TTG GGT GCA AT-3′and 5′-TTC CGG TGA GAG GTC CGG TT-3′ for VEGF, 5′-GAT TCC CAT ACC AAG TGT GCC-3′ and 5′-ATG TGG CGG AAG TAG TTC CC-3′for vasohibin-1, and 5′-CATCACCATCTTCCAGGAGC-3′ and 5′-CATGAGTCCTTCCACGATACC-3′ for GAPDH. All data were normalized to the GAPDH expression level, thus giving the relative expression level.

40.2.4 Western Blot Analysis for Vasohibin-1 and VEGF

Cells were collected and used for western blotting analysis after sonication, as we reported previously (Abe et al. 2008). Cells were washed in ice-cold Dalbecco's phosphate buffered saline (DPBS) 3 times, and then immediately sonicated in lysis buffer. After blotting on Immune-Blot PVDF Membrane (BIO-RAD Laboratories, CA), it was incubated overnight in mouse antivasohibin-1 or anti-VEGF antibody (Santa Cruz) at 4°C and visualized using an enhanced chemiluminescence system (ECL Plus, GE Healthcare) according to the manufacturer's instructions.

40.3 Results

40.3.1 Vasohibin-1 Expression

Vasohibin-1 expression in the RPE was confirmed by real-time PCR and western blot analysis. When we cultured the cells with cobalt chloride, a pseudo-hypoxic condition, or low oxygen (2%), 1% serum, and no glucose, gradual upregulation of VEGF gene was observed with 100-μM cobalt chloride (Fig. 40.1a). Conversely, statistically significant low vasohibin-1 expression was observed with 100-μM cobalt chloride at more than 12-h culture when compared to those of standard culture or less than 6-h culture (Fig. 40.1b). Western blot analysis showed that vasohibin-1 expression seemed to be downregulated at more than 36-h culture with 100-μM cobalt chloride (Fig. 40.1c).

40.3.2 RPE Dynamics and Proliferation by Vasohibin-1

An RTCA was used to monitor dynamic changes in the properties of RPE cells during the culture. The parameter of CI shows cell viability, number, morphology, and adhesion to the bottom of the plates. When we cultured the cells under standard condition as described above, we found no difference of CI even though we added VEGF (Fig. 40.2a) and/or vasohibin-1 (Fig. 40.2b). When we added VEGF (0.2–10 nM) in the culture medium at 2% oxygen, 1% serum, and no glucose, we found that VEGF enhanced CI (Fig. 40.2c). Statistically significant difference was observed when we cultured the cells more than 15 h after treatments with 1 and 2-nM VEGF.

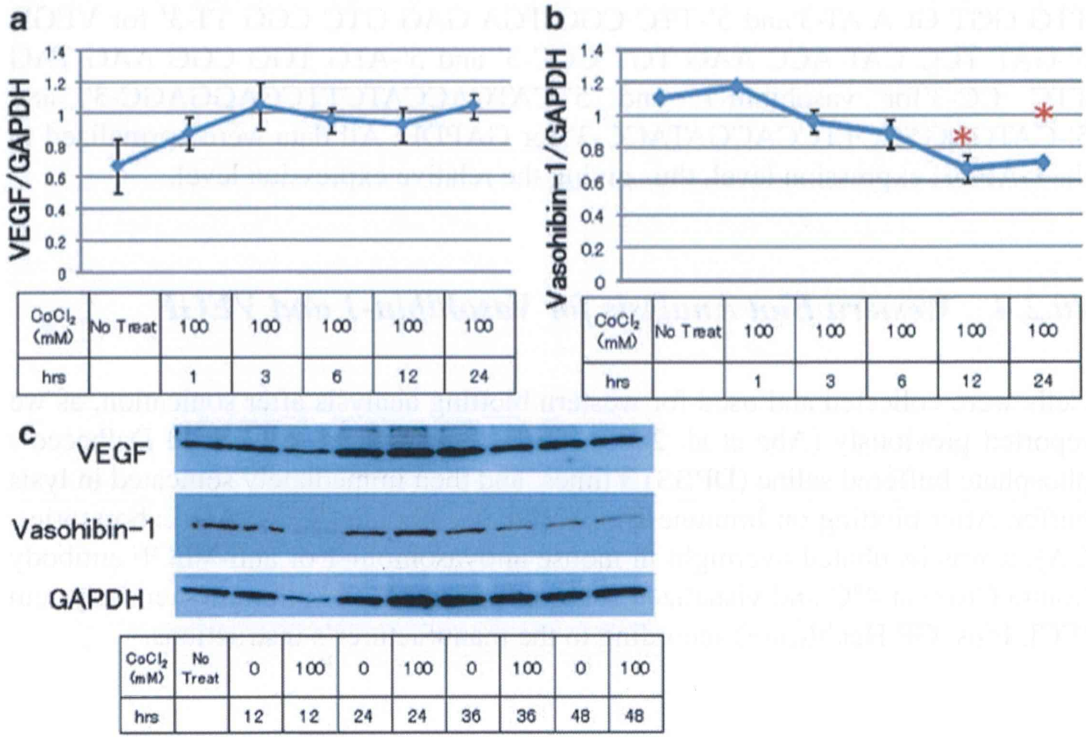

Fig. 40.1 Real-time PCR of VEGF (**a**) and vasohibin-1 (**b**) genes is shown. VEGF gene was upregulated in RPE-J with cobalt chloride during successive culture whereas vasohibin-1 gene was suppressed. Western blot analysis (**c**) shows decreased vasohibin-1 expression at the condition

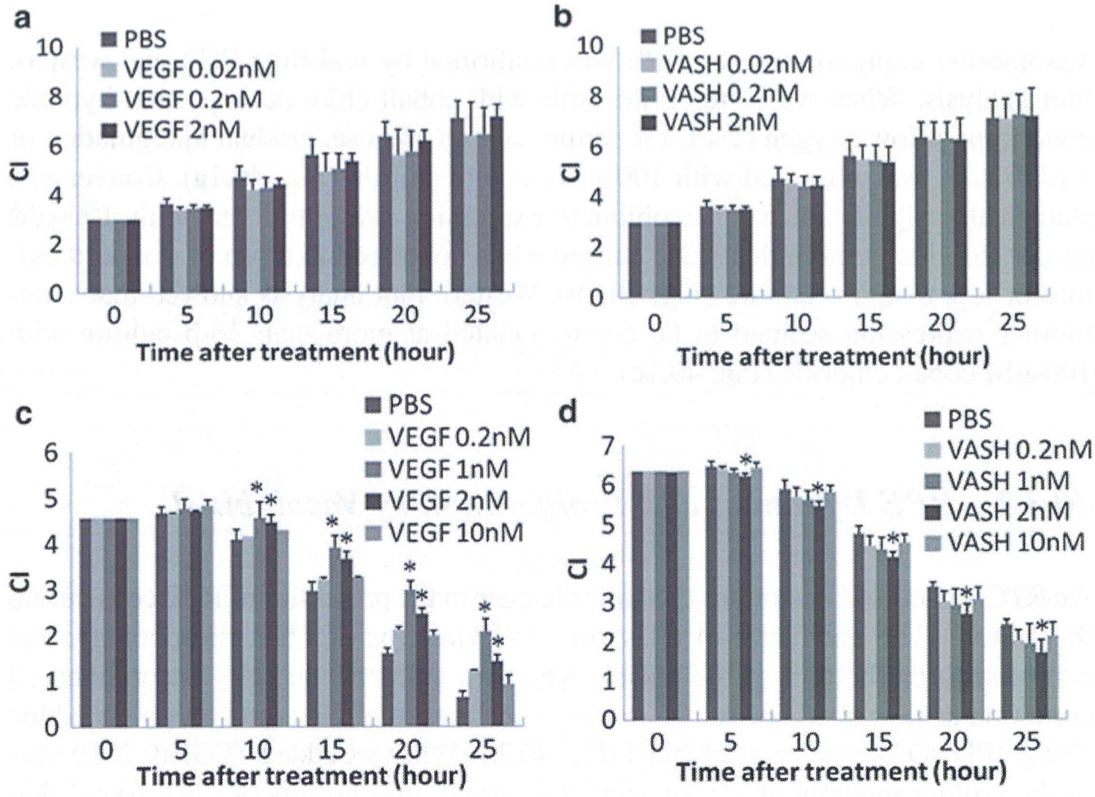

Fig. 40.2 Cell Index of RTCA shows that VEGF enhanced CI at hypoxic condition (**a**), conversely vasohibin-1 reduced CI only at hypoxic condition (**b**). The results were not observed at normal condition

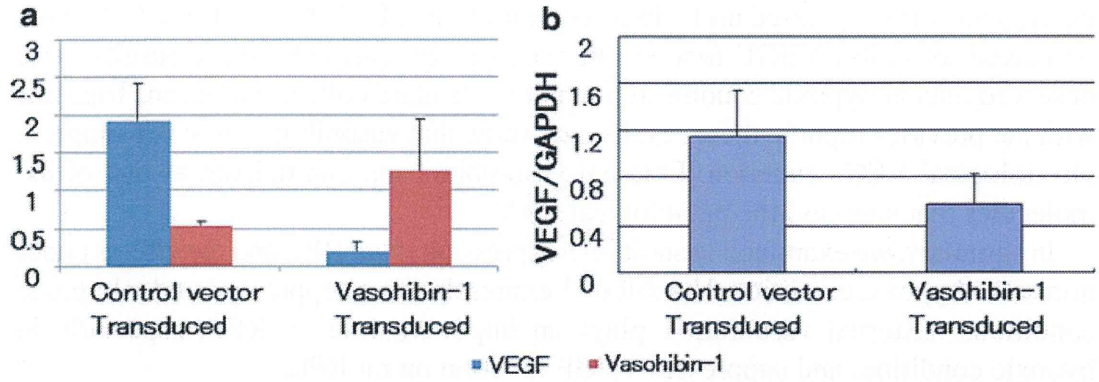

Fig. 40.3 Human vasohibin-1 gene was transduced into RPE-J. We selected 18 clones on both vasohibin-1 gene transduced and only vector-transduced RPE-J. Statistically significant less VEGF gene expression was observed in vasohibin-1 gene-transduced cDNA when compared to that of vector-transduced cDNA (**a**). Western blot analysis also showed comparable results (**b**)

Conversely, when we applied vasohibin-1 (0.2–10 nM) in the culture medium at 2% oxygen, 1% serum, and no glucose, we found that vasohibin-1 showed lower CI (Fig. 40.2d). Statistically significant difference was observed at 2-nM vasohibin-1. Vasohibin-1 application also showed statistically significant small cell number either 300-μM cobalt chloride or 2% oxygen, 1% serum, and no glucose. When we performed MTS assay, statistically significant less cell proliferation was also observed at these indicated conditions. When we examined the apoptotic cells, there was no significant difference. Human vasohibin-1 gene-transduced RPE-J showed statistically significant less VEGF expression when compared to those of vector-transduced cell by real-time PCR and western blot analysis (Fig. 40.3a, b).

40.4 Discussion

Vasohibin-1 is an endogenous antiangiogenic agent that is induced by variable pro-angiogenic factors such as VEGF and bFGF. Vasohibin-1 was reported to inhibit the sprouting of new vessels and to support vascular maturation processes (Kimura et al. 2009). These antiangiogenic properties were detected after recombinant vasohibin-1 was used for corneal and retinal neovascularization (Watanabe et al. 2004). We have found that vasohibin-1 is expressed on ECs of choroidal and retinal vessels, human CNV membranes (Wakusawa et al. 2008), and proliferative membranes of diabetic retinopathy (Sato et al. 2009). In addition, we suggested that the vasohibin-1/VEGF ratio was related to the activity of the CNV (Wakusawa et al. 2008). RPE is known for secreting VEGF from its basal side to choriocapillaris direction and performs important function for the survival of the vascular ECs and nonvascular cells developmentally and also in adults (Alon et al. 1995). This mechanism also maintains low VEGF concentration at subretinal space (Peng et al. 2010). Because of this specific function, we examined the correlation of vasohibin-1 and VEGF on RPE. From the results of present study, vasohibin-1 was expressed in RPE and the

expression was suppressed under hypoxic condition in RPE-J. Vasohibin-1 was also suspected to inhibit VEGF function of rat RPE. Interestingly, these results were observed only at hypoxic conditions and not in standard culture condition. Together with the previous reports, these results may show that vasohibin-1 may not suppress physiological VEGF function. External vasohibin-1 may participate as one of the molecules that suppress the pathological CNV.

In summary, we examined vasohibin-1 expression in rat RPE and the effects under normal or hypoxic condition. Vasohibin-1 expression was suppressed under hypoxic conditions. External vasohibin-1 plays an important role on RPE, especially in hypoxic condition, and suppresses VEGF function on rat RPE.

Acknowledgments This study was supported in part by grants from Grants-in-Aid for Scientific Research 20592030, 21592214 from the Japan Society for the Promotion of Science, Chiyoda-ku, Tokyo, Japan and Suzuken Memorial Foundation.

References

Abe T, Wakusawa R, Seto H et al (2008) Topical doxycycline can induce expression of BDNF in transduced retinal pigment epithelial cells transplanted into the subretinal space. Invest Ophthalmol Vis Sci 49: 3631–3639

Alon T, Hemo I, Itin A et al (1995) Vascular endothelial growth factor acts as a survival factor for newly formed retinal vessels and has implications for retinopathy of prematurity. Nat Med 1: 1024–1028

Bressler NM, Bressler SB, Fine SL (1998) Age-related macular degeneration. Surv Ophthalmol 32: 375–413

Kimura H, Miyashita H, Suzuki Y et al (2009) Distinctive localization and opposed roles of vasohibin-1 and vasohibin-2 in the regulation of angiogenesis. Blood 113: 4810–4818

Krzystolik MG, Afshari MA, Adamis AP et al (2002) Prevention of experimental choroidal neovascularization with intravitreal anti-vascular endothelial growth factor antibody fragment. Arch Ophthalmol 120: 338–346

Lux A, Llacer H, Heussen FMA et al (2007) Non-responders to bevacizumab (Avastin) therapy of choroidal neovascular lesions. Am J Ophthalmol 91: 1318–1322

Peng S, Adelman RA, Rizzolo LJ (2010) Minimal effects of VEGF and anti-VEGF drugs on the permeability or selectivity of RPE tight junctions. Invest Ophthalmol Vis Sci 51: 3216–33225

Pilli S, Kotsolis A, Spaide RF et al (2008) Endophthalmitis associated with intravitreal anti-vascular endothelial growth factor therapy injections in an office setting. Am J Ophthalmol 145: 879–882

Rosenfeld PJ, Brown DM, Heier JS et al (2006) MARINA Study Group. Ranibizumab for neovascular age-related macular degeneration. N Engl J Med 355: 1419–1431

Sato H, Abe T, Wakusawa R et al (2009) Vitreous levels of vasohibin-1 and vascular endothelial growth factor in patients with proliferative diabetic retinopathy. Diabetologia 52: 359–361

Sonoda H, Ohta H, Watanabe K et al (2006) Multiple processing forms and their biological activities of a novel angiogenesis inhibitor vasohibin. Biochem Biophys Res Commun 342: 640–646

Spilsbury K, Garrett KL, Shen WY et al (2000) Overexpression of vascular endothelial growth factor (VEGF) in the retinal pigment epithelium leads to the development of choroidal neovascularization. Am J Pathol 157: 135–144

Wakusawa R, Abe T, Sato H et al (2008) Expression of vasohibin, an antiangiogenic factor, in human choroidal neovascular membranes. Am J Ophthalmol 146: 235–243

Watanabe K, Hasegawa Y, Yamashita H et al (2004) Vasohibin as an endothelium-derived negative feedback regulator of angiogenesis. J Clin Invest 114: 898–907

Electrochemistry
The Electrochemical Society of Japan
Received: November 16, 2011
Accepted: February 4, 2012
Published: May 5, 2012
http://dx.doi.org/10.5796/electrochemistry.80.318
JOI:JST.JSTAGE/electrochemistry/80.318
Communication
Electrochemistry, **80(5)**, 318–320 (2012)

An Oxygen Responsive Microparticle-Patterned Hydrogel Sheet for Enzyme Activity Imaging

Kuniaki NAGAMINE,[a,b] Shuntaro ITO,[a] Mai TAKEDA,[a] Shingo OTANI,[a] and Matsuhiko NISHIZAWA[a,b,*]

[a] *Department of Bioengineering and Robotics, Graduate School of Engineering, Tohoku University, 6-6-01 Aramaki, Aoba-ku, Sendai 980-8579, Japan*
[b] *JST-CREST, Sanbancho, Chiyoda-ku, Tokyo 102-0075, Japan*

* *Corresponding author: nishizawa@biomems.mech.tohoku.ac.jp*

ABSTRACT
A patch-type oxygen imaging sheet useful for in vitro cellular metabolic assays was developed. Oxygen-responsive fluorescent microbeads were embedded into a biocompatible polyacrylamide gel sheet, which can be directly attached onto target cells for fluorescent imaging of metabolic activity. The sensor beads were directed in a microfluidic device using AC and DC electric manipulation techniques, followed by encapsulation in a hydrogel. Fluorescent imaging of oxygen-consuming activity was demonstrated for glucose oxidase-modified microparticles as cellular models to show the applicability of the imaging sheet to bioassays.

Keywords : Electrohydrodynamics, Microfluidic Device, Oxygen Imaging Sheet

1. Introduction

In vitro bioassays of cellular metabolic activity have been carried out to investigate the cell physiology. Evaluation of the oxygen-consuming activity of cells is significant for the indirect investigation of glucose metabolic activity. Such oxygen sensing would be applicable for revealing the mechanism of controlling blood glucose homeostasis and pathogenesis of type 2 diabetes using an insulin-responsive skeletal muscle cell.

In recent years, 2D fluorescent imaging sheets have been actively developed for mapping metabolite distribution in tissues.[1–4] In particular, Wolfbeis et al.[2,3] showed the applicability of pH- and oxygen-responsive sheets in animal experiments. All previous work used sheets in which the sensor microparticles were uniformly dispersed. However, the metabolite diffusion area is confined to the immediate vicinity of the cells. Besides, uniformly dispersed particles modify the characteristics of the hydrogel such as flexibility and nutrient permeability,[5] which will affect muscle cellular contractility and metabolic activity. In this study, the sensor beads were localized on the surface of the imaging sheet using AC and DC electric manipulation techniques to increase the surface sensitivity without sacrificing the merits of original gel characteristics. Fluorescent imaging of oxygen-consuming activity was demonstrated for glucose oxidase (GOD)-modified particles as cellular models (Fig. 1). When GOD-catalyzed glucose oxidation consumes the oxygen, the fluorescent intensity of the sensor beads increases in a pattern representing GOD activity.

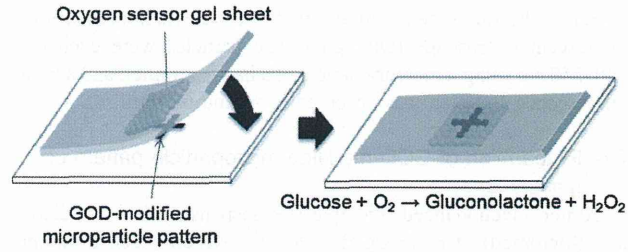

Figure 1. Schematic view of oxygen imaging around the pre-patterned GOD-modified microparticles.

2. Experimental

2.1 Preparation of oxygen responsive microparticles

A 3.5 mL of aqueous polystyrene microparticle suspension (1.0 μm diameter, Micromod) was mixed with 1.5 mL of tetrahydrofuran (THF) under ultrasonication for 10 min to swell the particles. A 0.5 mL solution of oxygen responsive fluorescent dye, platinum octaethylporphyrin (PtOEP, Sigma-Aldrich), dissolved in dimethyl sulfoxide was added to the particle suspension followed by another 20 min ultrasonication to incorporate the PtOEP into the particles.[6] Then, THF in the mixture was evaporated for 12 h at room temperature. The particles were separated by centrifugation, and washed two times with ethanol.

2.2 Fabrication of the microfluidic device

The microfluidic device was composed of three layers; an ITO top layer, a silicone rubber middle layer, and an ITO bottom layer covered with a negative photoresist SU-8 3005 pattern as an insulator. The silicone rubber layer had a stenciled opening that became the interior of the microchannel when sandwiched between the top and bottom ITO layers. The resulting microchannel was 10 mm in width and 500 μm in height. The channel inlet was connected to the particle suspension reservoir, and its outlet was attached to a syringe pump (World Precision Instruments) to introduce the particles into the channel.

2.3 Fabrication of the oxygen imaging sheet

The oxygen-responsive microparticles suspended in 0.5 mM NaCl solution were injected into the microchannel, and a sinusoidal AC voltage (100 Hz, 10 Vpp) was applied between the top and bottom ITO electrodes (Fig. 2A). The resulting AC electric field is strongest on the surface of the bottom ITO electrode, and the electrohydrodynamic force induces particle motion toward the bottom ITO pattern (1 mm × 1 mm). Then, the power supply was

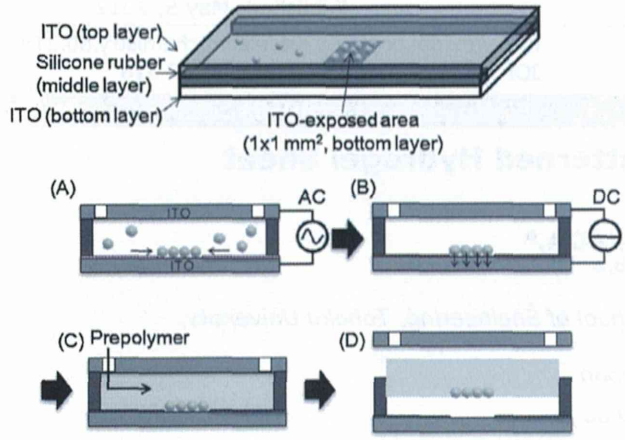

Figure 2. Preparation of the hydrogel sheet with patterned oxygen-responsive microparticles.

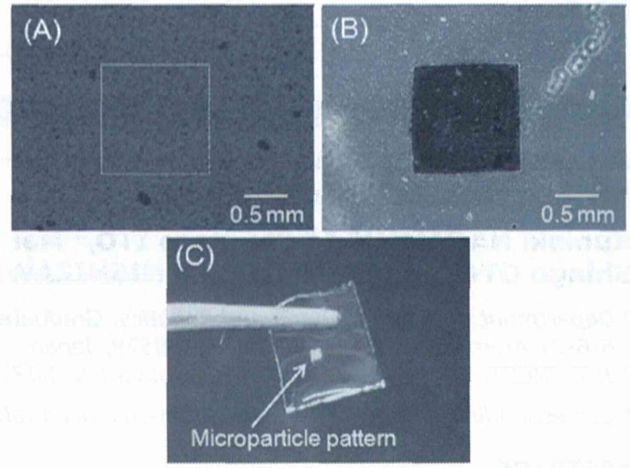

Figure 3. (A, B) Phase contrast micrographs (A) before and (B) after application of AC voltage between the top and bottom ITO electrodes. White-dashed line in (A) represents the ITO pattern on the bottom of the microchannel. (C) Photograph of the polyacrylamide hydrogel sheet with the oxygen responsive microparticle pattern embedded.

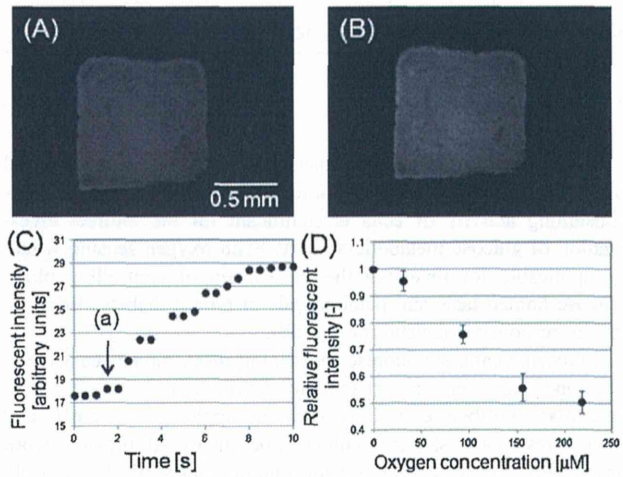

Figure 4. (A, B) Fluorescent images of the oxygen responsive microparticles in PBS(−) at a dissolved oxygen concentration of (A) 185 μM and (B) 0 μM. (C) Typical time-course of the fluorescent intensity change when Na_2SO_3 solution was added into PBS(−) at point (a). (D) Relationship between the relative fluorescent intensity of the imaging sheet and the dissolved oxygen concentration. Oxygen concentration was controlled by gradually adding Na_2SO_3 solution into the previously air-bubbled PBS(−). Each point represents the mean of three measures ± SD.

switched to 2.0 V DC to fix the patterned particles on the bottom ITO surface (Fig. 2B). After flushing out any unattached particles, the 20% (w/v) acrylamide and 1% (w/v) bis-acrylamide monomers including 0.4 vol% ammonium persulfate and 0.1 vol% tetramethylethylenediamine were injected into the channel. The device was left undisturbed for 2 h at room temperature to facilitate gelation (Fig. 2C).[7] The resulting sheet was cut into square (10 mm × 10 mm). The fluorescence of the particles was monitored using a fluorescent microscope (Olympus). The particles were excited at 520–550 nm using a mercury lamp and a bandpass filter, and a broad fluorescence emission was observed at around 650 nm.

2.4 Preparation of GOD-modified microparticle pattern on a glass substrate

Amino-functionalized microparticle suspension (1.0 μm diameter, Micromod) was dropped onto the stencil-attached amino-silanized glass substrate and evaporated overnight. The stencil sheet (100 μm thick) has a cross-formed line pattern (line width: 300 μm) made by a cutting plotter (Graphtech). An 8% glutaraldehyde solution was poured onto the particles for 1 h at room temperature to covalently immobilize the particles on the substrate and to functionalize the residual amines on the particles with glutaraldehyde. After washing away the unreacted glutaraldehyde, 1 mg/mL GOD (Wako Pure Chemicals Co.) suspended in PBS(−) (pH 7.0) was poured onto the particles and reacted at 4°C overnight to covalently immobilize the GOD onto the particles. By peeling off the stencil, the GOD-modified microparticle pattern was left on the substrate. 50 mM D-glucose dissolved in PBS(−) was dropped onto the GOD pattern to previously initiate the glucose oxidation. Then, the oxygen imaging sheet was put on the GOD pattern to obtain fluorescent image of oxygen-consuming activity.

3. Results and Discussion

Figure 3 shows snapshots over time of the microparticle patterning using electrohydrodynamic force. Microparticles were introduced into the microchannel to be monodispersed (Fig. 3A). Upon application of the AC electric field, the particles rapidly moved toward the exposed ITO rectangular pattern (Fig. 3B). As demonstrated by several researchers, the application of a low frequency AC electric field drives the particles to move in a direction transverse to the field (toward the bottom ITO electrode pattern) via electrohydrodynamic fluid flow, and the particles accumulate in a two-dimensional ordered structure near the electrode surface.[8] Then, the power supply was switched to DC voltage to immobilize the negatively-charged polystyrene particles on the electrode during the solution change from water to a polyacrylamide prepolymer. Figure 3C shows a photograph of the polyacrylamide hydrogel sheet embedded with the rectangular-shaped sensor particle pattern. The particle transfer efficiency from the ITO electrode surface to the hydrogel was almost 100%.

Figure 4A shows fluorescent images of the oxygen-responsive particles on the hydrogel immersed in PBS(−) dissolving 185 μM oxygen. Oxygen-responsive dye, PtOEP, encapsulated into the particles is based on the ability of molecular oxygen to quench the dye selectively.[9] Therefore, the fluorescent intensity increases as the oxygen concentration decreases. As expected, when Na_2SO_3